RAA 2019 Vol. **19** No. **10**, 150(12pp) doi: 10.1088/1674–4527/19/10/150

http://www.raa-journal.org *http://iopscience.iop.org/raa*

Research in Astronomy and Astrophysics

The abundance of massive compact galaxies at $1.0 < z < 3.0$ in 3D-*HST*/CANDELS

Shi-Ying Lu[1], Yi-Zhou Gu[1], Guan-Wen Fang[2] and Qi-Rong Yuan[1]

[1] Department of Physics and Institute of Theoretical Physics, Nanjing Normal University, Nanjing 210023, China; *yuanqirong@njnu.edu.cn*

[2] Institute for Astronomy and History of Science and Technology, Dali University, Dali 671003, China; *wen@mail.ustc.edu.cn*

Received 2018 December 25; accepted 2019 May 29

Abstract Based on a large sample of massive ($M_* \geqslant 10^{10}\,M_\odot$) compact galaxies at $1.0 < z < 3.0$ in five 3D-*HST*/CANDELS fields, we quantify the fractional abundance and comoving number density of massive compact galaxies as a function of redshift. The samples of compact quiescent galaxies (cQGs) and compact star-forming galaxies (cSFGs) are constructed by various selection criteria of compact galaxies in the literature, and the effect of compactness definition on abundance estimate has proven to be remarkable, particularly for the cQGs and cSFGs at high redshifts. Regardless of the compactness criteria adopted, their overall redshift evolutions of fractional abundance and number density are found to be rather similar. Large samples of the cQGs exhibit a sustained increase in number density from $z \sim 3$ to 2 and a plateau at $1 < z < 2$. For massive cSFGs, a plateau in the number density at $2 < z < 3$ can be found, as well as a continuous drop from $z \sim 2$ to 1. The evolutionary trends of the cQG and cSFG abundances support the scenario that the cSFGs at $z \gtrsim 2$ may have been rapidly quenched into quiescent phase via violent dissipational processes, such as major merger and disk instabilities. The rarity of the cSFGs at lower redshifts ($z < 1$) can be interpreted by the decrease of gas reservoirs in dark matter halos and the consequent low efficiency of gas-rich dissipation.

Key words: galaxies: high-redshift — galaxies: massive — compact — galaxies: evolution — galaxies

1 INTRODUCTION

It has been widely appreciated that there has been a bimodality in galaxy populations, i.e., blue star-forming galaxies (SFGs) vs. red quiescent galaxies (QGs), since the universe was only ~2.5 Gyr old (Strateva et al. 2001; Kauffmann et al. 2003a,b; Baldry et al. 2004; Blanton & Moustakas 2009; Brammer et al. 2009; Whitaker et al. 2011, 2012; Huertas-Companyal et al. 2015). Therefore, it is believed that there should be an evolutionary connection between the two populations. A picture of star formation quenching has proposed that the SFGs would truncate their star formation activities and transform into a quiescent status (Blanton et al. 2003; Brinchmann et al. 2004; Kauffmann et al. 2004; Faber et al. 2007; Peng et al. 2010; Fang et al. 2012; Barro et al. 2013, 2014; Gu et al. 2018). Many large surveys (such as the SDSS, NMBS, UltraVISTA, zFOURGE and CANDELS) have provided the probability to study the physical processes and mechanisms relevant to star formation quenching over a wide span of cosmic time.

The observational link between quenching and structure properties has increasingly come to attention. In general, the SFGs are found to have an extended structure, with larger non-circularized effective radii (r_e) than the QGs (e.g., Williams et al. 2009; Fang et al. 2012; van der Wel et al. 2012; Whitaker et al. 2012; Cassata et al. 2013; van der Wel et al. 2014; Huertas-Companyal et al. 2015). The QGs in the early epoch are three to five times more compact than their local counterparts (Newman et al. 2010; Bruce et al. 2012; Ryan et al. 2012; Cassata et al. 2013). Moreover, van der Wel et al. (2014) report that early-type galaxies (ETGs) at fixed stellar mass follow a faster size evolution, $r_\mathrm{e} \propto (1+z)^{-1.48}$, while late-type galaxies (LTGs) manifest a slower evolution in size, $r_\mathrm{e} \propto (1+z)^{-0.75}$. Compact quiescent galaxies (cQGs, also called "red nuggets") are found to be ubiquitous at $z \sim 2$ (Damjanov et al. 2009). A similar population of compact star-forming galaxies (cSFGs, also called "blue nuggets") is confirmed to be present at high redshifts (Barro et al. 2013, 2014; Fang et al. 2015; van Dokkum et al. 2015). However, in the local universe, massive compact galaxies are quite rare, with the number density on the order of $10^{-6}\,\mathrm{Mpc}^{-3}$ (Trujillo et al. 2009; Taylor et al. 2010; Trujillo et al. 2014; Graham et al. 2015; Saulder et al. 2015; Buitrago et al. 2018) but which are preferentially found in galaxy clusters (Valentinuzzi et al. 2010; Poggianti et al. 2013a,b; Peralta de Arriba et al. 2016).

Why the abundances of compact galaxies are discrepant at different redshifts and how these massive compact galaxies form and evolve are still unsolved issues. Some mechanisms are proposed to explain the formation and evolution of these compact galaxies. SFGs with extended structures (called extended SFGs, eSFGs for short) are believed to be the progenitors of massive compact galaxies (Barro et al. 2013, 2014; Fang et al. 2015; van Dokkum et al. 2015). This suggests that the cSFGs are formed from the eSFGs by shrinking their sizes via violent gas-rich dissipational processes (Dekel et al. 2013; Dekel & Burkert 2014; Zolotov et al. 2015). On account of the high luminosities of star formation or active galactic nucleus (AGN) activities triggered by gas-rich dissipational processes, the cSFGs would consume their cool gas rapidly, and soon evolve to cQGs (Barro et al. 2013; Fang et al. 2015; Tadaki et al. 2015). Furthermore, these cQGs could evolve to local massive QGs or extended quiescent galaxies (eQGs) through minor mergers later (Hopkins et al. 2010; de la Rosa et al. 2016). Ultimately, the majority of these massive compact galaxies at $z \sim 2$ ends up in the central dense cores of local galaxies (van Dokkum et al. 2014; Belli et al. 2014).

Although the compact galaxy population covering a wide range of redshift has been studied by many investigators (e.g., $z \lesssim 1.0$: Trujillo et al. 2009, 2014; Saulder et al. 2015; Zahid et al. 2015; Charbonnier et al. 2017; $z \gtrsim 1.0$: Barro et al. 2014; Cassata et al. 2013; Fang et al. 2015; van der Wel et al. 2014; van Dokkum et al. 2015), the statistical results of massive compact galaxies are rather diverse, which is mainly due to different observational data and different strategies in the selection of compact galaxies. For example, Charbonnier et al. (2017) and Damjanov et al. (2019) applied the same criteria for compact galaxies to the CFHT Stripe 82 (CS82) survey and the Subaru Hyper Suprime-Cam (HSC) high-resolution imaging survey, respectively. Their cosmic evolution of cQG number densities since $z \sim 0.4$ is different from each other. Even with the same data, the statistics of massive compact galaxies (i.e., cQGs and cSFGs) will be severely biased when we adopt different thresholds of stellar mass, effective radius and compactness in sampling. For instance, an abundance of cSFGs in the CANDELS fields at higher redshifts ($z \gtrsim 1.0$) has been estimated by Barro et al. (2014) and Fang et al. (2015) with different compactness criteria, and their results also differ.

To untangle the effect of different compactness criteria, it is necessary to make a comprehensive comparison for the samples of cSFGs and cQGs at higher redshifts that are selected with different criteria. In this paper, we will compile a large sample of massive $(M_* \geqslant 10^{10}\,M_\odot)$ galaxies at $1.0 < z < 3.0$ in the five deep fields of the 3D-*HST*/CANDELS programs (Grogin et al. 2011; Koekemoer et al. 2011; Skelton et al. 2014). All of the massive galaxies are separated into quiescent and star-forming populations using the rest-frame UVJ diagram (Williams et al. 2009). Then, eight different criteria of compact galaxies in the literature (Carollo et al. 2013; Quilis & Trujillo 2013; Barro et al. 2014; van der Wel et al. 2014; Fang et al. 2015; van Dokkum et al. 2015) will be adopted to construct the samples of cQGs and cSFGs. For these various samples of cSFGs and cQGs, their fractional abundances and number densities can be computed as a function of redshift. A detailed comparison between these results can tell us how the different criteria affect the conclusions about fractional abundance and number density of cQGs and cSFGs.

The rest of this paper is organized as follows. We give an overview of the 3D-*HST*/CANDELS data set and a description of our sample selection in Section 2, including various criteria of compact galaxies. In Section 3, we present the evolution of the fraction and number density of massive compact galaxies, and further discuss the evolutionary connection between cSFGs and cQGs. Finally, we give a summary in Section 4. Throughout the paper, we assume the cosmology model with $\Omega_\mathrm{M} = 0.3$, $\Omega_\Lambda = 0.7$ and $\mathrm{H}_0 = 70\,\mathrm{km\,s}^{-1}\,\mathrm{Mpc}^{-1}$.

2 DATA AND SAMPLE SELECTION

2.1 Data Description

On the basis of high-quality WFC3 and ACS spectroscopy and multi-wavelength photometry in the five 3D-*HST*/CANDELS fields (i.e., AEGIS, COSMOS, GOODS-N, GOODS-S and UDS) (Grogin et al. 2011; Koekemoer et al. 2011; Skelton et al. 2014), we set about selecting a large sample of massive galaxies. The database is from CANDELS and 3D-*HST* Treasury programs including the WFC3 *F*125*W*, *F*140*W*, *F*160*W* images (Skelton et al. 2014), which have been observed with many other space- and ground-based telescopes. The total area of the five fragmented deep fields is ∼900 arcmin^2, which can mitigate the influence of cosmic variance to a certain extent.

The photometric redshifts (z_phot) and the rest-frame UVJ colors are derived by Skelton et al. (2014) with the

EAZY code (Brammer et al. 2008). The derived photometric redshifts for the five CANDELS fields have higher precision, and their normalized median absolute deviations ($\sigma_{\rm NMAD}$), defined as $\sigma_{\rm NMAD} = 1.48 \times$ median[$\mid \triangle z - {\rm median}(\triangle z)|/(1+z)$], are within a range from 0.007 (COSMOS) to 0.026 (GOODS-N) (Skelton et al. 2014). In this paper, we preferentially adopt the spectroscopic redshifts ($z_{\rm spec}$) if available. The stellar masses are derived by Skelton et al. (2014), who fit the spectral energy distribution (SED) using the FAST code (Kriek et al. 2009) based on the Bruzual & Charlot (2003) stellar population synthesis (SPS) models with Chabrier (2003) initial mass function (IMF) and solar metallicity. Additionally, van der Wel et al. (2012) estimated the non-circularized effective radius $r_{\rm e}$ and axis ratio q by applying the GALFIT code (Peng et al. 2002). We adopt the GALFIT results of J band ($F125W$) images for the galaxies at $1.0 < z \leqslant 1.8$, and H band ($F160W$) results for the galaxies at $1.8 < z < 3.0$, for ensuring the structural feature is observed with the same optical band in the rest frame. The axis ratio q can be taken to calculate the non-circularized effective radius, a key parameter in some definitions of compactness (see Sect. 2.3).

2.2 Sample of Massive QGs and SFGs

First, based on the multi-wavelength photometric data in five 3D-*HST*/CANDELS fields, we select a large sample of 7767 massive galaxies ($M_* \geqslant 10^{10}\,M_\odot$) with good photometric quality (i.e., `use_phot=1`) and good morphological fits with GALFIT (i.e., GALFIT flag $=$ 0 or1) at $1.0 < z < 3.0$ to ensure high sample completeness and robust structural measurements. The completeness above the mass threshold is around $\sim 90\%$ up to the highest redshift (Grogin et al. 2011; Wuyts et al. 2011; Newman et al. 2012; Barro et al. 2013; Pandya et al. 2017). Figure 1 displays the scatterplot and histograms of stellar mass and redshift.

To investigate the evolution of the number density of cSFGs and cQGs, respectively, we divide our sample into QGs and SFGs by utilizing the rest-frame UVJ diagram. Many previous works have suggested that the UVJ diagram can be employed to distinguish QGs from dusty SFGs, even at higher redshifts $z \sim 3$ (Wuyts et al. 2007; Williams et al. 2009; Brammer et al. 2009; Whitaker et al. 2011, 2012; Muzzin et al. 2013; van der Wel et al. 2014; Huertas-Companyal et al. 2015). The criteria for selecting QGs are provided below (Williams et al. 2009)

$$(U-V) > 0.88 \times (V-J) + 0.49\,, \tag{1}$$

$$(U-V) > 1.3\,, \tag{2}$$

$$(V-J) < 1.6\,. \tag{3}$$

In Figure 2, the rest-frame UVJ diagrams (i.e., U $-$ V vs. V $-$ J) are exhibited for four redshift bins with an interval of $\Delta z = 0.5$. As a result, 5832 SFGs and 1935 QGs with $M_* \geqslant 10^{10}\,M_\odot$ at $1.0 < z < 3.0$ are picked for the subsequent selection of compact galaxies.

2.3 Compactness Criteria

In the recent literature, final results about the abundance of compact galaxies depend heavily on the definition of compactness. There are many versions of compactness criteria which are dramatically different. One of our objectives is to untangle the effect of different compactness criteria on the abundance of massive compact galaxies. Therefore, the various criteria of compact galaxies are addressed in this subsection.

It is necessary to describe the structural parameters adopted in the definition of compactness. To quantify the size of galaxies, the non-circularized effective radius $r_{\rm e}$, defined as the semi-major axis in arcsec of the ellipse that contains half of the total light, can be estimated by fitting with the Sérsic model (van der Wel et al. 2012). The circularized effective radius, $r_{\rm e,c}$, can be derived by the following formula

$$r_{\rm e,c} = r_{\rm e} \times \sqrt{q}\,, \tag{4}$$

where q means the axis ratio, i.e., $q = b/a$. Both $r_{\rm e}$ and $r_{\rm e,c}$ are in units of kpc in this paper. The size-mass relations for our sample of massive galaxies in four redshift bins are presented in Figure 3. In general, the SFGs have larger sizes than the QGs in all redshift bins. Linear fittings are performed for both massive SFGs and QGs. In both cases, their sizes tend to become larger over cosmic time (i.e., from high to low redshifts). Similar results have been shown in recent works (Daddi et al. 2005; Whitaker et al. 2012; Huertas-Companyal et al. 2015; Gu et al. 2018; Damjanov et al. 2019). Compared with the SFGs, massive QGs at $1 < z < 3$ are found to have smaller sizes that are more dependent on the stellar mass. Slopes of the size-mass relation for the early-type quiescent population are steeper than those for SFGs, which are in good agreement with van der Wel et al. (2014).

The *Gini* coefficient, as a nonparametric measurement, has been taken to exclude some cSFGs with visually extended structures by Fang et al. (2015). As described in Abraham et al. (2003) and Lotz et al. (2004), the *Gini* coefficient is defined to quantify the relative distribution of pixel fluxes

$$Gini = \frac{\sum_l^N (2l-N-1) \mid F_l \mid}{\overline{F} N(N-1)}, \tag{5}$$

where F_l is the pixel flux value sorted in ascending order, $\overline{F}$ is the mean pixel flux and N is the total number of pixels

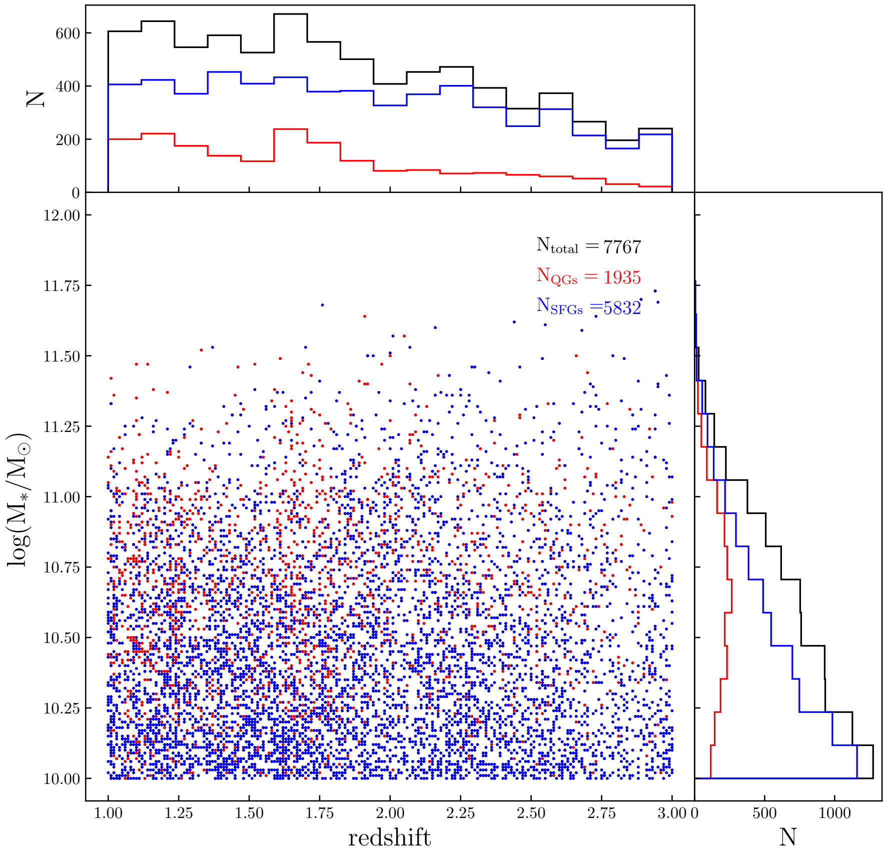

Fig. 1 Distribution of massive galaxies in the five CANDELS fields in the stellar mass – redshift plane. All of the massive galaxies (*black dots*/*curves*) are separated by the UVJ diagram (see Sect. 2.2 and Fig. 2) into QGs (*red dots*/*curves*) and SFGs (*blue dots*/*curves*). The corresponding numbers are displayed at the top-right corner.

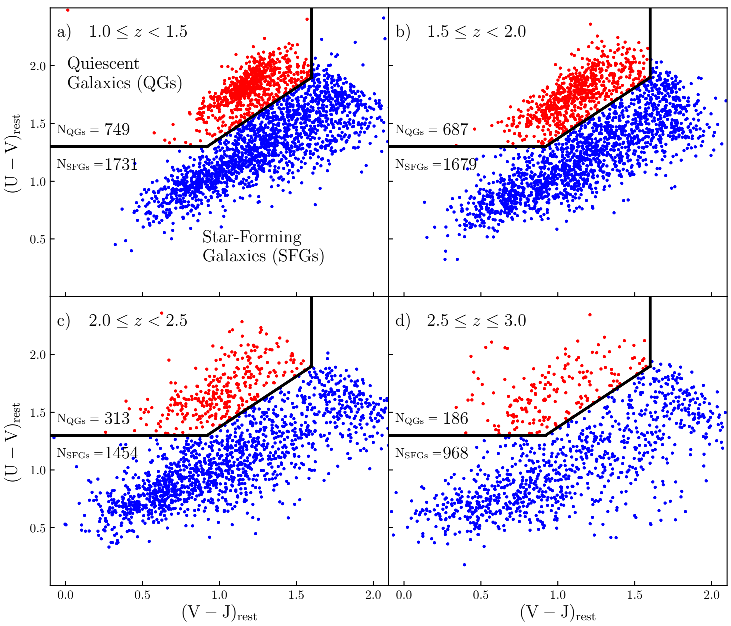

Fig. 2 The rest-frame UVJ diagram for massive galaxies in four redshift bins. The *solid black lines*, following the criteria from Williams et al. (2009), separate massive galaxies into QGs (*red dots*) and SFGs (*blue dots*). The numbers of QGs and SFGs are shown near the horizontal boundaries.

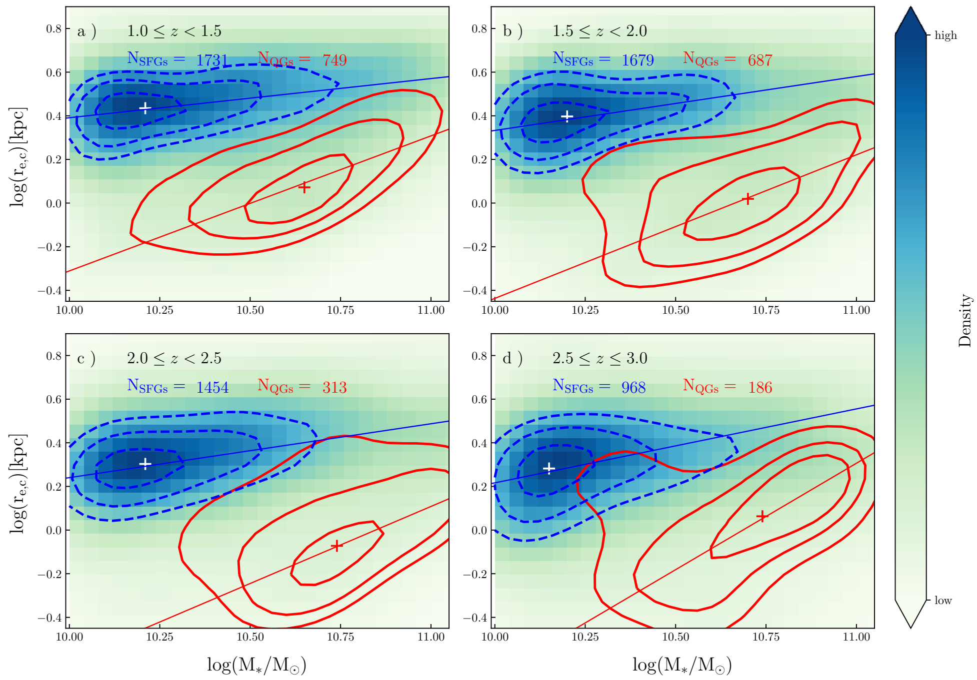

Fig. 3 The size of a galaxy as a function of stellar mass in four redshift bins. The *color blocks* represent the relative density in the size-mass relation. The contour levels for SFGs (in *blue*) and QGs (in *red*) trace the 10%, 30% and 50% of grid counts with densities sorted in descending order. *Blue* and *red solid lines* indicate the linear fittings for two inner contours. The median values of circularized effective radius and stellar mass for the samples of SFGs (in *white*) and QGs (in *red*) are marked with *crosses*. The numbers of SFGs and QGs are also given at the top.

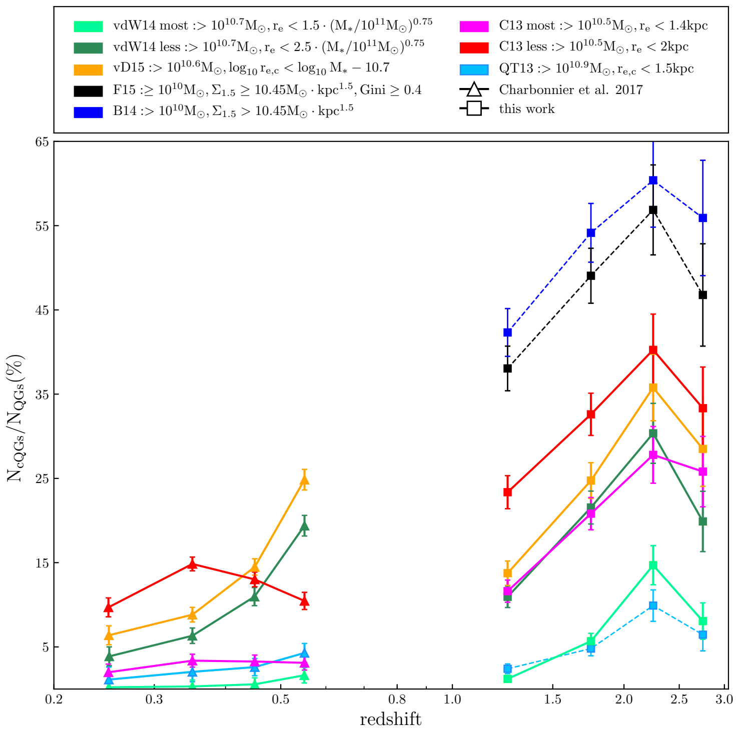

Fig. 4 The redshift evolution of the cQG fractional abundance (i.e., the ratio of the number of massive cQGs to that of massive QGs) in a wide range of redshift ($0.2 < z < 3.0$). The abbreviations and specific criteria of the cQGs listed in Table 1 are shown at the top of the figure, distinguished by different colors. The data points at high redshifts ($1 < z < 3$), marked with *squares*, represent the results for our eight samples of cQGs. The results at low redshifts ($0.2 < z < 0.6$) by Charbonnier et al. (2017) are also signified with triangles.

Table 1 Various Definitions of Compactness and the Sizes of Our cQG and cSFG Samples

No.	Mass limit	Compactness criteria	Number of cQGs	Number of cSFGs	Abbreviations[a]
1	$> 10^{10.5}\,M_\odot$	the "*most*" compact $r_{\rm e} < 1.4\,{\rm kpc}$	365	100	C13 most
2	$> 10^{10.5}\,M_\odot$	the "*less*" compact $r_{\rm e} < 2.0\,{\rm kpc}$	587	217	C13 less
3	$> 10^{10.9}\,M_\odot$	$r_{\rm e,c} < 1.5\,{\rm kpc}$	94	37	QT13
4	$> 10^{10}\,M_\odot$	${\Sigma_{1.5}}^{\rm b} > 10.45\,M_\odot\,{\rm kpc}^{1.5}$	982	455	B14
5	$> 10^{10.7}\,M_\odot$	the "*most*" compact $r_{\rm e} < 1.5 \times (M_*/10^{11}\,M_\odot)^{0.75}$	109	47	vdW14 most
6	$> 10^{10.7}\,M_\odot$	the "*less*" compact $r_{\rm e} < 2.5 \times (M_*/10^{11}\,M_\odot)^{0.75}$	362	192	vdW14 less
7	$\geqslant 10^{10}\,M_\odot$	${\Sigma_{1.5}}^{\rm b} \geqslant 10.45\,M_\odot\,{\rm kpc}^{1.5}$ and *Gini* $\geqslant 0.4$	887	360	F15
8	$> 10^{10.6}\,M_\odot$	$\log_{10}(r_{\rm e,c}) < \log_{10}(M_*/M_\odot) - 10.7$	438	250	vD15

a: The different criteria are expressed by abbreviations. (C13: Carollo et al. 2013; QT13: Quilis & Trujillo 2013; B14: Barro et al. 2014; vdW14: van der Wel et al. 2014; F15: Fang et al. 2015; vD15: van Dokkum et al. 2015). The 'most' and 'less' represent the most and less compact criteria as it applies respectively.
b: The $\Sigma_{1.5}$ is a *pseudo*-stellar mass surface density, defined as $\log_{10}(M_*/r_{\rm e,c}^{1.5})$ (Barro et al. 2013).

belonging to a galaxy. The *Gini* coefficient can be regarded as a generalized measure of concentration. Moreover, it is able to describe the arbitrary shape of a galaxy without requiring a single well-defined nucleus (i.e, multiple cores). In this work, the *Gini* coefficients are measured by the version of Morpheus software developed by Abraham et al. (2007).

We collect all of the specific definitions of compact galaxies that have been adopted in recent works. These definitions take different lower limits of stellar mass and different size cuts. The specific compactness criteria are listed in Table 1, as well as the number counts of our cQG and cSFG samples at $1 < z < 3$ for each compactness definition.

3 THE ABUNDANCE OF MASSIVE COMPACT GALAXIES

3.1 The Fractional Abundance

To demonstrate the effect of the definition of compactness on the cQG and cSFG abundance at high redshifts, we adopt eight different definitions of compact galaxies (see Table 1) to select the cQGs and cSFGs at $1 < z < 3$ in the 3D-*HST*/CANDELS fields. Fractional abundance of the cQGs (cSFGs) is defined as the ratio of the number of cQGs (cSFGs) to total number of QGs (SFGs).

Compared with Charbonnier et al. (2017) and Damjanov et al. (2019), we adopt more criteria to differentiate compact galaxies from massive QGs and SFGs, and the corresponding counts of cQGs and cSFGs are reported in Table 1. Figure 4 plots the fractional abundances of eight cQG samples at high redshifts which are selected by different compactness criteria. It is found that the cQG fractions in the QG samples tend to increase with redshift at $z \gtrsim 2.0$, then decrease rapidly at $z < 2$. Although the different compactness criteria are adopted, the overall variations of the cQG fraction with redshift are similar.

To observe the cosmic evolution of the cQG fraction from $z \sim 3$ to 0.2, the fractional abundances at $0.2 < z < 0.6$ which were derived by Charbonnier et al. (2017) are also presented in the same diagram. Compared with results from the above two works, in which the criteria from Carollo et al. (2013) (C13 most: magenta lines and C13 less: red lines) are applied, the fractional abundances of the cQGs tend to be fewer from $z \sim 1.0$ to 0.6. The cQG fraction seems to increase when the sizes of compact galaxies are related to stellar masses (vdW14 less; vD15). By comparing the evolutionary trends between low and high redshifts, the influence by different compactness criteria on the cQG fraction cannot be ignored over the blank range of redshift. Furthermore, for the two criteria in Quillis & Trujillo (2013) (QT13: dodger blue lines) and in van der Wel et al. (2014) (vdW14 most: spring green lines), the cQG fractions have a slight change from $z \sim 1.0$ to 0.6 because of the strict selection of compact galaxies (i.e., a higher mass threshold $M_* > 10^{10.7}\,M_\odot$ and a small upper limit of size). It should be mentioned that the diversity of the cQG fraction due to different criteria adopted is found to be larger at $z > 1.0$ (even up to $\sim 50\%$) than that at $0.2 < z < 0.6$ (Charbonnier et al. 2017). However, the overall redshift evolution of cQG fraction at $1 < z < 3$ is similar.

Compared with cQG fraction, the situation for redshift evolution of cSFG fractions is rather different, as shown in Figure 5. A simple rising trend along redshift can be found for cSFG fractional abundances at $1 < z < 3$, except for the criterion (F15: black dashed line) from Fang et al. (2015). The trend discontinues at $z > 2$ in Fang et al. (2015) when the *Gini* coefficient is adopted to get rid of some cSFGs with extended structure at high redshifts. The rising slopes in the diagram of fractional abundance vs. redshift are dependent upon the criteria of compactness.

Regardless of the difference in compactness definition, the fractional abundance of cSFGs is found to be much higher at high redshifts ($z > 2$) than that at lower redshifts ($z \lesssim 1$). According to some predictions by simulation, cSFGs are formed by gas-rich, dissipational processes, such as cold accretion from the intergalactic medium

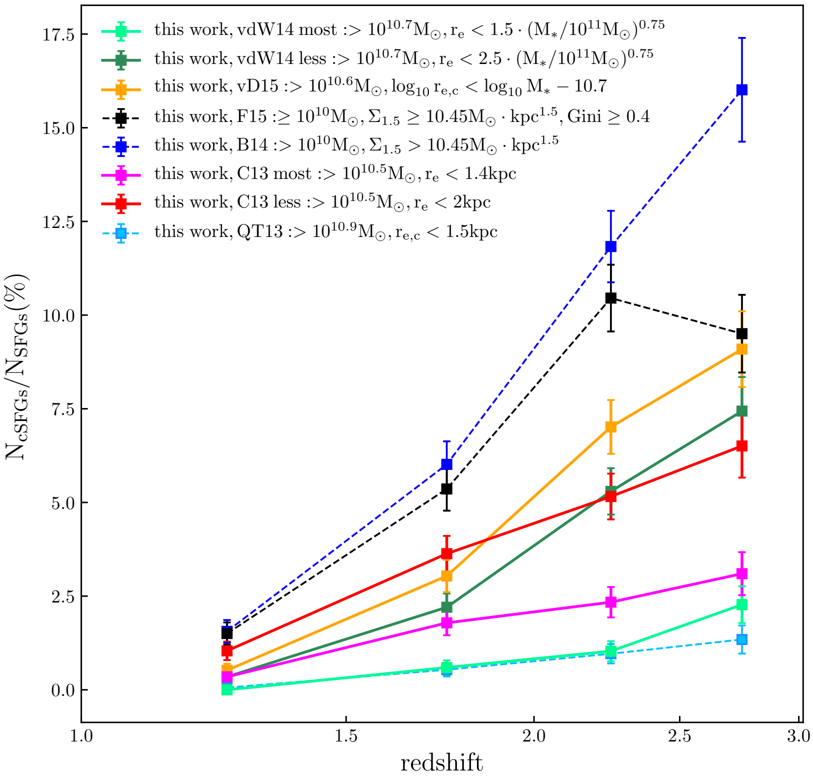

Fig. 5 The redshift evolution of fractional abundance of cSFGs between 1.0 and 3.0. The indications of colors and symbols are the same as in Fig. 4.

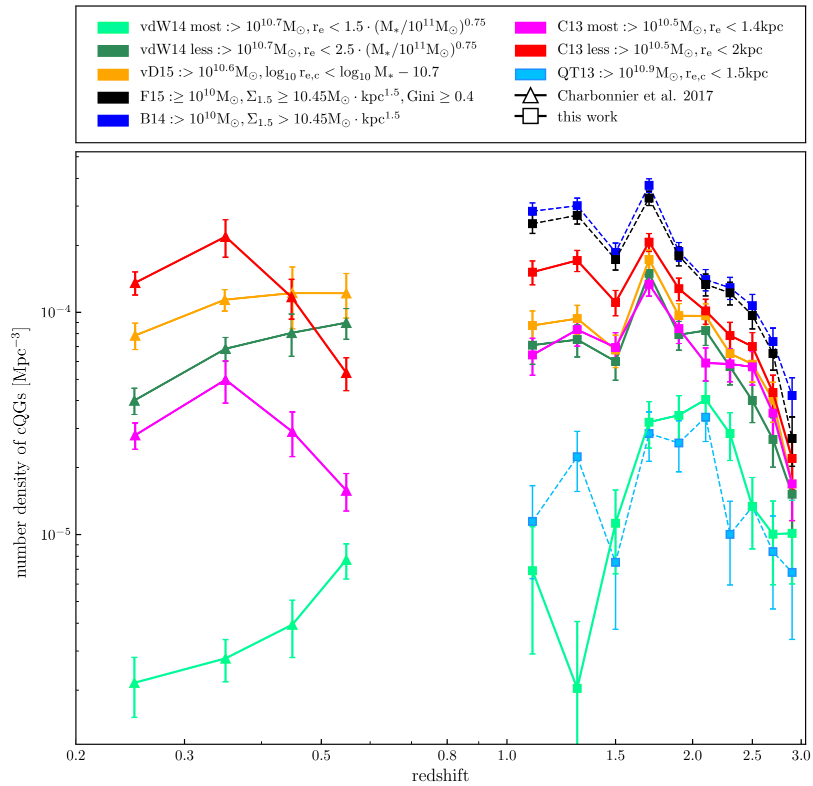

Fig. 6 The redshift distribution of number density of cQGs compared our observed cQGs (*squares*) at $z \geqslant 1.0$ with the ones (*triangles*) compiled from Charbonnier et al. (2017) at $z < 0.6$. Different colors indicate different definitions of compactness. The indications of colors and symbols are the same as in Fig. 4.

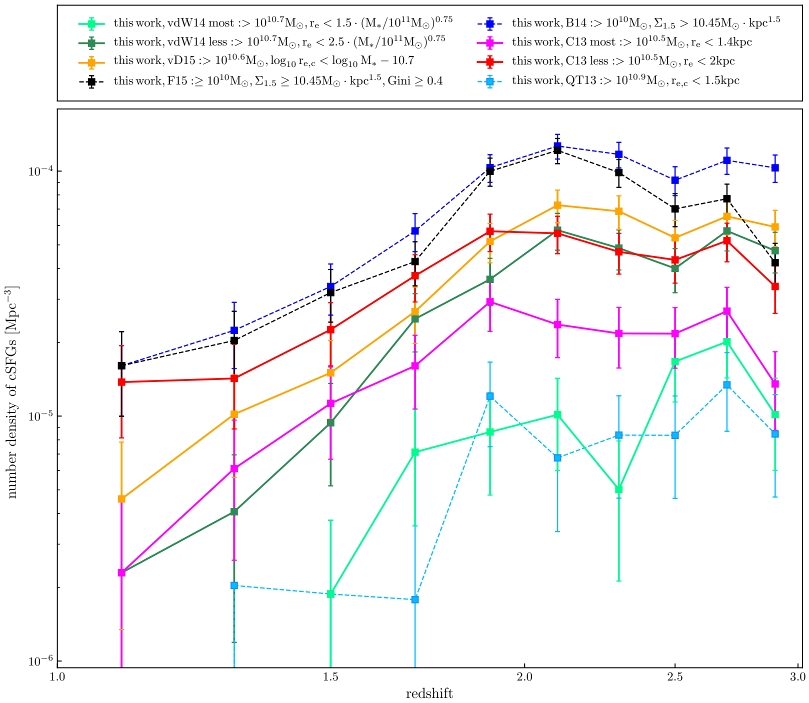

Fig. 7 The redshift evolution of number density for cSFGs at $1 < z < 3$. All the results are based on our samples in five 3D-*HST*/CANDELS fields. The indications of colors and symbols are the same as in Fig. 4.

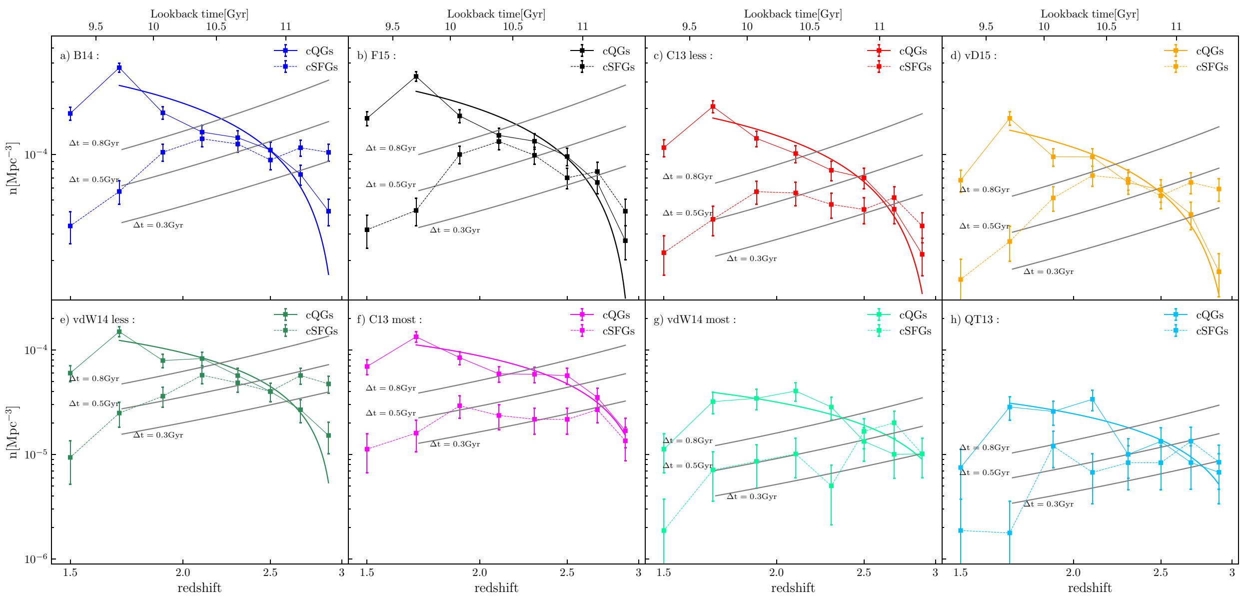

Fig. 8 The redshift evolutions of number density for the massive cQGs (*solid*) and cSFGs (*dotted*) selected by eight different compactness criteria. Different colors signify different compactness criteria, and the corresponding abbreviations are shown at the top. The corresponding solid curve is the best fit to the cQG number density in each panel. The *solid gray lines* depict the evolutions of cSFG number density which are required to match the observed increasing cQG number density, following Barro et al. (2013). The corresponding lifetimes of cSFGs and the lookback times (*in the top row*) are also shown.

(IGM) via violent disk instability (Dekel et al. 2009a,b), cold mode accretion (Birnboim & Dekel 2003; Johansson et al. 2012) and major mergers (Hopkins et al. 2009, 2010; Wuyts et al. 2010). Star formation in the cSFGs is subsequently quenched by some feedbacks such as AGN feedback (Barro et al. 2013, 2014; Kocevski et al. 2017) and stellar winds driven by intense starbursts (Tremonti et al. 2007; Heckman et al. 2011). Kocevski et al. (2017) find that 39.2% of massive cSFGs host an X-ray detected AGN, which is higher than the incidence of AGN in eSFGs, indicating that AGN feedback helps to decrease the number density of cSFGs. Therefore, these feedback mechanisms imprint evidence that extremely rare cSFGs are found at lower redshifts $0.5 < z < 1$ (Trujillo et al. 2009; Taylor et al. 2010; Barro et al. 2013; Trujillo et al. 2014). Compactness can be treated as a very sensitive predictor of passivity among massive galaxies, particularly at higher redshifts (Bell et al. 2012; Williams et al. 2014).

By synthesizing the cosmic evolution of fractional abundances of cQGs and cSFGs, the connection between cQGs and cSFGs can be discussed. If we adopt a simple evolutionary model (Barro et al. 2013) (see Sect. 3.2 and Fig. 8), it can be found that the lifetimes of cSFGs at high redshift selected by different compactness criteria are less than 0.8 Gyr, which are in agreement with Barro et al. (2013, 2014) and van Dokkum et al. (2015). Based on the number densities of green valley galaxies and QGs at $0.5 < z < 2.5$ in the fields of CANDELS, Gu et al. (2019) estimated the upper limit of the average transition/quenching timescale as a function of redshift, and the average quenching timescale at $z \sim 2.5$ is less than 0.35 Gyr. The fractional abundance for the cQGs peaks at $z \sim 2.0$, which can be construed by the assumption that a certain percentage of cSFGs at $z \gtrsim 2$ may have been quenched into the cQGs via a rapid violent dissipational process (Barro et al. 2013; Fang et al. 2015; Williams et al. 2015). The average quenching timescale becomes longer than 1.3 Gyr since $z \sim 2$, and the accumulative effects from the above-mentioned feedback mechanisms and minor mergers during longer passive evolution may result in a looser stellar distribution in the massive QGs (Gu et al. 2019). This picture may help us to understand the declining trend in the cQG fractional abundance since $z \sim 2$.

3.2 Number Density Evolution

It has been widely appreciated that massive cSFGs will rapidly quench into cQGs at high redshifts (Barro et al. 2013; Fang et al. 2015; van Dokkum et al. 2015). However, the opposite path of evolution in which the cQGs begin their star formation activities via accreting new gas has also be proposed (so-called “rejuvenation”) (Graham et al. 2015; Zolotov et al. 2015). For investigating the evolution of massive compact galaxies at high redshifts, we further quantify the comoving number densities of the cQGs and cSFGs within a small interval of $\Delta z = 0.2$. The number density can be determined by dividing the number of massive compact galaxies by its comoving volume within the redshift interval. The correction to number density is not adopted in our work due to the high completeness at high redshift (see Sect. 2.2). In contrast, if we follow the method adopted by Charbonnier et al. (2017), then the real results will be blurred at higher redshift in terms of more obvious disadvantage of double Schechter function at the low mass end (Ilbert et al. 2013).

Figure 6 presents the number densities of the cQGs in five 3D-*HST*/CANDELS fields at $1 < z < 3$, as well as the results compiled from the CS82 data at $0.2 < z < 0.6$ by Charbonnier et al. (2017), which are uncorrected by completeness factors. Except for two cQG samples (vdW14 most: spring green and QT13: dodger blue lines) selected with a higher mass threshold ($M_* > 10^{10.7}\,M_\odot$) and a small upper limit of size, the remaining six samples include at least 300 cQGs, and their number densities are more statistically reliable. For these large samples of cQGs at $1 < z < 3$, their redshift evolutions of the cQG number densities are quite similar, exhibiting a sustained increase from $z \sim 3$ to 2 and a maximum density at $z \sim 1.8$. This trend is consistent with the results in previous works (Cassata et al. 2011, 2013; Barro et al. 2013; van der Wel et al. 2014; van Dokkum et al. 2014, 2015). For the cQGs at $1 < z < 2$, the cQG number density tends to be constant, with a typical number density of $\sim 10^{-4}\,\mathrm{Mpc}^{-3}$.

Compared to the cQG number densities by Charbonnier et al. (2017), we find that the number densities of the less compact samples of van der Wel et al. (2014) and Carollo et al. (2013) are on average 0.4 and 0.2 dex higher than their number density under most compactness criteria at $1 < z < 3$, which are smaller than the deviation values of number density between less and most compact criteria compiled from Charbonnier et al. (2017). From Figure 6, the difference in number density between less and most compact definition (e.g., vdW14 less and most) is obviously getting bigger with decreasing redshift ($1 < z < 3$), which is likely to be due to the decrease in number of massive compact galaxies satisfying criteria with higher mass threshold. The bigger error bars with decreasing redshift may reflect more obvious influence of cosmic variance on lower redshift . Moreover, if we take a lower mass threshold (i.e., $M_* \gtrsim 10^{10.5}\,M_\odot$, Carollo et al. 2013), then a declining trend over cosmic time within the blank redshift range (i.e., from $z \sim 1.0$ to 0.6) can be inferred, which agrees with Barro et al. (2013), van der Wel et al. (2014), van Dokkum et al. (2015) and Cassata et al. (2013) (for ultra-compact ETGs). However, for the other cQG definitions with higher mass thresholds (i.e., $M_* \gtrsim 10^{10.6}\,M_\odot$, van der Wel et al. 2014; van Dokkum et al. 2015), constant number densities can be expected at $0.6 < z < 1.0$, which are consistent with Cassata et al. (2013) (for compact ETGs) and Gargiulo et al. (2016) (for ultramassive dense ETGs). A moderate decrease in the cQG number density since $z \sim 1$ can be interpreted with the early-track described in Barro et al. (2013), where some cQGs transform into eQGs through a minor merger as also mentioned by Gargiulo et al. (2016). Naab et al. (2009) performed hydrodynamic cosmological simulations of the formation of massive galaxies to demonstrate that a minor merger may be the main driver for evolution in sizes and densities of massive ETGs, which is in agreement with Oser et al. (2012) where dry minor mergers come to be predominant since $z \sim 2$ instead of major mergers alone. The rarity of cSFGs since $z \sim 1$ (see Fig. 7) results in a very low consequent birth rate of the cQGs at lower redshifts.

The redshift evolution of cSFG number density is also presented in Figure 7. Regardless of various cSFG selection criteria, the redshift evolution of the cSFG number density is very similar: keeping a constant number density at $2 < z < 3$ and a continuous decline from $z \sim 2$ to 1. Our results are consistent with those in Barro et al. (2013) and van Dokkum et al. (2015). When taking the definition from Fang et al. (2015), a significant hump at $z \sim 2$ can be found in Figure 7. Owing to taking *Gini* coefficient into consideration, a substantial fraction of the cSFGs at $z > 2$ with clear extended structures may have been excluded by this strict criterion (see fig. 5 in Fang et al. 2015).

It is worth considering whether the compact galaxy number density is sensitive to the stellar mass threshold (e.g., QT13: mass limit $> 10^{10.9}\,M_{\odot}$). Damjanov et al. (2015) find that the compactness threshold or the stellar mass range has no significant impact on the compact galaxy number density over the redshift range $0.2 < z < 0.8$. To check whether the mass limits influence abundance of compact galaxies at higher redshifts ($1 < z < 3$), two extreme cases of mass thresholds ($> 10^{10.9}$ and $\geqslant 10^{10}\,M_{\odot}$) are adopted in all compactness definitions. It is found that all evolutionary trends of compact galaxies (cQGs in Figs. 4, 6 and cSFGs in Figs. 5, 7) are not sensitive to the mass thresholds. Certainly, a higher mass threshold and a strict compactness criterion will lead to fewer numbers of compact galaxies being selected.

The evolutionary scenario between cQGs and cSFGs can be speculated upon based on both the redshift evolutions of number density. Figure 8 presents the difference in number density evolution between the cQGs and cSFGs at $z \gtrsim 2$. If we adopt a simple evolutionary model proposed by Barro et al. (2013) in which all cSFGs will become quiescent after experiencing a short starburst phase, a crude explanation can be derived for the discrepancy in number density between cQGs and cSFGs. A plateau in the cSFG number density at $2 < z < 3$ can be explained by the balance between birth rate of new cSFGs via rapid gas-rich dissipational process (such as major merger and disk instabilities) and quenching rate of the cSFGs. The quenching of cSFGs at $z \gtrsim 2$ will surely lead to a strong increase in the number density of cQGs from $z \sim 3$ to 1.7. As shown in Figure 8, it is found that the corresponding lifetimes of cSFGs are approximately $\Delta t_{\rm burst} \sim 0.3-0.8\,$Gyr. Barro et al. (2013) and van Dokkum et al. (2015) compared the redshift evolution between the cSFGs and cQGs as well, and estimated the timescale of quenching via central starburst feedback. They referred to an average quenching timescale below 1 Gyr as the lifetime of cSFGs, which is consistent with our timescale estimate, ($\Delta t_{\rm burst} \sim 0.3 - 0.8\,$Gyr), for different compactness criteria in this work. By using semi-analytic models of galaxy formation, Barro et al. (2014) suggest that cSFGs would have to end their lives with an abrupt decline in the star formation rate (SFR) on a short timescale ($t_{\rm q} \sim 400\,$Myr), and then reproduce the emergence of the quiescent population. Moreover, for the cSFGs with higher compactness, Figure 8 demonstrates that the timescale of current burst of star formation tends to be shorter. The drop in the cSFG number density since $z \sim 1.8$ will lead to a plateau in the cQG number density at $1.0 < z < 1.7$ since no new cQGs are added to the sample. Due to the lower SFR toward decreasing redshift as predicted by some simulations (Finlator et al. 2007; Tonini et al. 2012; Barro et al. 2014), cSFGs are not formed in large numbers at $z < 2$ in the late-track described by Barro et al. (2013), and some QGs are supplied by the quenching of eSFGs. The abundances of cSFGs rapidly drop from $z \sim 2$ to 1, which can be interpreted by the decrease of gas reservoirs in dark matter halos (Croton 2009; Geach et al. 2011) and the consequent low efficiency of gas-rich dissipation (Barro et al. 2013). The decline in the abundances of cSFGs in this work corresponds to the decrease of gas-rich major merger rate for massive SFGs since $z \sim 1.8$ derived by López-Sanjuan et al. (2013).

4 SUMMARY

In this paper, a large sample of massive galaxies with $M_* \geqslant 10^{10}\,M_{\odot}$ at $1 < z < 3$ in five 3D-*HST*/CANDELS fields has been separated into quiescent and star-forming populations by the rest-frame UVJ diagram. We further select the cQGs and cSFGs using eight different definitions of compactness in the literature (Carollo et al. 2013; Quilis & Trujillo 2013; Barro et al. 2014; van der Wel et al. 2014; Fang et al. 2015; van Dokkum et al. 2015). To explore the evolutionary connection between the cQGs and cSFGs, fractional abundance and number density are quantified as a function of redshift. The main conclusions are summarized as follows:

1. We confirm that massive QGs are on average smaller than massive SFGs in size at $1 < z < 3$. For a specified redshift range, the slope of the size-mass relation

is steeper for massive QGs. The sizes of massive QGs are much more dependent on stellar mass than those of massive SFGs.

2. We adopt eight different definitions of compact galaxies to select cQGs and cSFGs at $1 < z < 3$. The effect of the compactness definition on the values of fractional abundance and comoving number density is remarkable for the cQG and cSFG samples. However, their evolutionary trends in the abundance of compact galaxies are found to be rather similar regardless of the adopted mass thresholds and specific compactness criteria.
3. For cQGs, both the fractional abundance and the number density of cQGs peak at $z \sim 2.0$. For the large samples of cQGs, their number densities exhibit a sustained increase from $z \sim 3$ to 2 and a plateau at $1 < z < 2$. Comparing with the results at $0.2 < z < 0.6$ from Charbonnier et al. (2017), a declining tend in number density over cosmic time is expected within the redshift gap (i.e., from $z \sim 1$ to 0.6) for the cQG samples with a lower mass threshold of $10^{10.5}\,M_{\odot}$. A constant cQG number density at $0.6 < z < 1$ can be inferred for the more massive cQGs with $M_{*} \gtrsim 10^{10.6}\,M_{\odot}$.
4. For cSFGs, a rising trend along redshift is found for fractional abundance at $1 < z < 3$, except for the compactness criterion with the *Gini* coefficient by Fang et al. (2015). A plateau in the number density at $2 < z < 3$ can be ascertained in the cSFG samples, as well as a continuous decline from $z \sim 2$ to 1.
5. Taking the abundances of both the cSFGs and cQGs at $1 < z < 3$ into consideration, their behaviors in redshift evolution favor the scenario in which a certain fraction of cSFGs at $z \gtrsim 2$ may have been quenched into the cQGs via rapid violent dissipational processes such as major mergers or disk instabilities, which lead to a remarkable increase in the cQG number density from $z \sim 3$ to 2. Rarity of the cSFGs at lower redshifts ($z < 1$) is due to the decrease of available gas in dark matter halos. A small fractional abundance for local cQGs ($z < 0.3$) may be due to the effect of size enlargement via minor mergers.

Acknowledgements This work is based on observations taken by the 3D-*HST* Treasury Program (GO 12177 and 12328) with the NASA/ESA *HST*, which is operated by the Association of Universities for Research in Astronomy, Inc., under NASA contract NAS5-26555. This work is supported by the National Natural Science Foundation of China (Nos. 11673004, 11873032 and 11433005) and by the Research Fund for the Doctoral Program of Higher Education of China (No. 20133207110006). G. W. F acknowledges the support from Yunnan young and middle-aged academic and technical leaders reserve talent program (No. 201905C160039).

References

Abraham, R. G., Nair, P., McCarthy, P. J., et al. 2007, ApJ, 669, 184
Abraham, R. G., van den Bergh, S., & Nair, P. 2003, ApJ, 588, 218
Baldry, I. K., Glazebrook, K., Brinkmann, J., et al. 2004, ApJ, 600, 681
Barro, G., Faber, S. M., Perez-Gonzalez, P. G., et al. 2013, ApJ, 765, 104
Barro, G., Faber, S. M., Péez-González, P. G., et al. 2014, ApJ, 791, 52
Bell, E. F., van der Wel, A., Papovich, C., et al. 2012, ApJ, 753, 167
Belli, S., Newman, A. B., & Ellis, R. S. 2014, ApJ, 783, 117
Blanton, M. R., Hogg, D. W., Bahcall, N. A., et al. 2003, ApJ, 594, 186
Blanton, M. R., & Moustakas, J. 2009, ARA&A, 47, 159
Brammer, G. B., Whitaker, K. E., van Dokkum, P. G., et al. 2009, ApJ, 706, L173
Brammer, G. B., van Dokkum, P. G., & Coppi, P. 2008, ApJ, 686, 1503
Birnboim, Y., & Dekel, A. 2003, MNRAS, 345, 349
Brinchmann, J., Charlot, S., White, S. D. M., et al. 2004, MNRAS, 351, 1151
Bruce, V. A., Dunlop, J. S., Cirasuolo, M., et al. 2012, MNRAS, 427, 1666
Bruzual, G., & Charlot, S. 2003, MNRAS, 344, 1000
Buitrago, F., Ferreras, I., Kelvin, L. S., et al. 2018, ArXiv: 1807.02534
Carollo, C. M., Bschorr, T. J., Renzini, A., et al. 2013, ApJ, 773, 112
Cassata, P., Giavalisco, M., Guo, Y., et al. 2011, ApJ, 743, 96
Cassata, P., Giavalisco, M., Williams, C. C., et al. 2013, ApJ, 775, 106
Chabrier, G. 2003, PASP, 115, 763
Charbonnier, A., Huertas-Company, M., Gonçalves, T. S., et al. 2017, MNRAS, 469, 4523
Croton, D. J. 2009, MNRAS, 394, 1109
Daddi, E., Renzini, A., Pirzkal, N., et al. 2005, ApJ, 626, 680
Damjanov, I., Geller, M. J., Zahid, H. J., et al. 2015, ApJ, 806, 158
Damjanov, I., McCarthy, P. J., Abraham, R. G., et al. 2009, ApJ, 695, 101
Damjanov, I., Zahid, H. J., Geller, M. J., et al. 2019, ApJ, 872, 91
de la Rosa, I. G., La Barbera, F., Ferreras, I., et al. 2016, MNRAS, 457, 1916
Dekel, A., Birnboim, Y., Engel, G., et al. 2009a, Nature, 457, 451
Dekel, A., Sari, R., & Ceverino, D. 2009b, ApJ, 703, 785
Dekel, A., Zolotov, A., Tweed, D., et al. 2013, MNRAS, 435, 999
Dekel, A., & Burkert, A. 2014, MNRAS, 438, 1870

Faber, S. M., Willmer, C. N. A., Wolf, C., et al. 2007, ApJ, 665, 265
Fang, G. W., Kong, X., Chen, Y., et al. 2012, ApJ, 751, 109
Fang, G. W., Ma, Z. Y., Kong, X., et al. 2015, ApJ, 807, 139
Finlator, K., Davé, R., & Oppenheimer, B. D. 2007, MNRAS, 376, 1861
Gargiulo, A., Saracco, P., Tamburri, S., et al. 2016, A&A, 592, A132
Geach, J. E., Smail, I., Moran, S. M., et al. 2011, ApJ, 730, L19
Graham, A. W., Dullo, B. T., & Savorgnan, G. A. D. 2015, ApJ, 804, 32
Grogin, N. A., Kocevski, D. D., Faber, S. M., et al. 2011, ApJS, 197, 35
Gu, Y. Z., Fang, G. W., Yuan, Q. R., et at. 2018, ApJ, 855, 10
Gu, Y. Z., Fang, G. W., Yuan, Q. R., et at. 2019, ApJ, in press, arxiv:1909.07103
Heckman, T. M., Borthakur, S., Overzier, R., et al. 2011, ApJ, 730, 5
Hopkins, P. F., Bundy, K., Croton, D., et al. 2010, ApJ, 715, 202
Hopkins, P. F., Cox, T. J., Younger, J. D., & Hernquist, L. 2009, ApJ, 691, 1168
Huertas-Company M., Pérez-González, P. G., Mei, S., et al. 2015, ApJ, 809, 95
Ilbert, Q., McCracken, H. J., Le Fèvre, O., et al. 2013, A&A, 556, A55
Johansson, P. H., Naab, T., & Ostriker, J. P. 2012, ApJ, 754, 115
Kauffmann, G., Heckman, T. M., Tremonti, C., et al. 2003b, MNRAS, 346, 1055
Kauffmann, G., Heckman, T. M., White, S. D. M., et al. 2003a, MNRAS, 341, 33
Kauffmann, G., White, S. D. M., Heckman, T. M., et al. 2004, MNRAS, 353, 713
Kocevski, D. D., Barro, G., Faber, S. M., et al. 2017, ApJ, 846, 112
Koekemoer, A. M., Faber, S. M., Ferguson, H. C., et al. 2011, ApJS, 197, 36
Kriek, M., van Dokkum, P. G., Labbé, I., et al. 2009, ApJ, 700, 221
López-Sanjuan, C., Fèvre, O. Le., Tasca, L. A. M., et al. 2013, A&A, 553, A78
Lotz, J. M., Primack, J., & Madau, P. 2004, AJ, 128, 163
Muzzin A., Marchesini, D., Stefanon, M., et al. 2013, ApJS, 206, 8
Naab, T., Johansson, P. H., & Ostriker, J. P. 2009, ApJ, 699, L178
Newman A. B., Ellis R. S., Bundy, K., & Treu, T. 2012, ApJ, 746, 162
Newman A. B., Ellis R. S., Treu T., & Bundy K. 2010, ApJ, 717, L103
Oser, L., Naab, T., Ostriker, J. P., et al. 2012, ApJ, 744, 63
Pandya, V., Brennan, R., Somerville, R. S., et al. 2017, MNRAS, 472, 2054
Peng, C. Y., Ho, L. C., Impey, C.D., & Rix, H-W. 2002, AJ, 124, 266
Peng, Y. J., Lilly, S. J., Kovač, K., et al. 2010, ApJ, 721, 193
Peralta de Arriba, L., Quilis, V., Trujillo, I., et al. 2016, MNRAS, 461, 156
Poggianti, B. M., Calvi, R., Bindoni, D., et al. 2013a, ApJ, 762, 77
Poggianti, B. M., Moretti, A., Calvi, R., et al. 2013b, ApJ, 777, 125
Quilis V., & Trujillo I. 2013, ApJ, 773, L8
Ryan Jr. R. E., McCarthy, P. J., Cohen, S. H., et al. 2012, ApJ, 749, 53
Saulder, C., van den Bosch, R. C. E., & Mieske, S. 2015, A&A, 578, A134
Skelton, R. E., Whitaker, K. E., Momcheva, I. G., et al. 2014, ApJS, 214, 24
Strateva, I.V., Ivezić, Ž., Knapp, G. R., et al. 2001, AJ, 122, 1861
Tadaki, K.-i., Kohno, K., Kodama, T., et al. 2015, ApJ, 811, L3
Tonini, C., Bernyk, M., Croton, D., Maraston, C., & Thomas, D. 2012, ApJ, 759, 43
Taylor, E. N., Franx, M., Glazebrook, K., et al. 2010, ApJ, 720, 723
Tremonti, C. A., Moustakas, J., & Diamono-Stanic, A. M. 2007, ApJ, 663, L77
Trujillo, I., Cenarro, A. J., Lorenzo-Cáceres, A. D., et al. 2009, ApJ, 692, L118
Trujillo, I., Ferré-Mateu, A., Balcells, M., et al. 2014, ApJ, 780, L20
Valentinuzzi, T., Fritz, J., Poggianti, B. M., et al. 2010, ApJ, 712, 226
van der Wel, A., Bell, E. F., Häussler, B., et al. 2012, ApJS, 203, 24
van der Wel, A., Franx, M., van Dokkum, P. G., et al. 2014, ApJ, 788, 28
van Dokkum, P. G., Bezanson, R., van der Wel, A., et al. 2014, ApJ, 791, 45
van Dokkum, P. G., Nelson, E. J., Franx, M., et al. 2015, ApJ, 813, 23
Whitaker, K. E., Labbé, I., van Dokkum, P. G.,et al. 2011, ApJ, 735, 86
Whitaker, K. E., Kriek M., van Dokkum P. G., et al. 2012, ApJ, 745, 179
Williams, R. J., Quadri R. F., Franx M., et al. 2009, ApJ, 691, 1879
Williams, C. C., Giavalisco, M., Cassata, P., et al. 2014, ApJ, 780, 1
Williams, C. C., Giavalisco, M., Lee, B., et al. 2015, ApJ, 800, 21
Wuyts, S., Cox, T. J., Hayward, C. C., et al. 2010, ApJ, 722, 1666
Wuyts, S., Förster Schreiber, N. M., van der Wel, A., et al. 2011, ApJ, 742, 96
Wuyts, S., Labbé, I., Franx, M., et al. 2007, ApJ, 655, 51
Zahid, H. J., Damjanov, I., Geller, M. J., & Chilingarian, I. 2015, ApJ, 806, 122
Zolotov, A., Dekel, A., Mandelker, N., et al. 2015, MNRAS, 450, 2327